DOI:
10.1088/0957-4484/27/28/285102

Document Version
Peer reviewed version

Targeted Lipid-Polyaniline Hybrid Nanoparticles for Photoacoustic Imaging Guided Photothermal Therapy of Cancer

Jinping Wang [a], Ran Yan [b], Fang Guo [a], Meng Yu [a], Fengping Tan [a,**], Nan Li [a,*]

[a] Tianjin Key Laboratory of Drug Delivery & High-Efficiency, School of Pharmaceutical Science and Technology, Tianjin University, Tianjin, PR China.

[b] Division of Imaging Sciences and Biomedical Engineering, King's College London, London, United Kingdom

**Co-corresponding author at: School of Pharmaceutical Science and Technology, Tianjin University, 300072, Tianjin, PR China.

E-mail address: tanfengping@163.com

Tel.:+86-022-27405160

*Corresponding author at: School of Pharmaceutical Science and Technology, Tianjin University, 300072, Tianjin, PR China.

Tel.:+86-022-27404986

E-mail address: linan19850115@163.com

Abstract

Designing a targeted and versatile photothermal agent for integration of precise diagnosis and effective photothermal treatment of tumors is desirable but remains a great challenge. In this study, folic acid ligand conjugated lipid coated polyaniline hybrid nanoparticles (FA-Lipid-PANI NPs) were successfully fabricated by a distinctive technology. The obtained hybrid FA-Lipid-PANI NPs with small size possessed not only significant photoaccoustic (PA) imaging signal but also remarkable photothermal effect for tumor treatment. With PA imaging and photothermal therapy (PTT), the tumor could be accurately positioned and thoroughly eradicated in vivo after intravenous injection of FA-Lipid-PANI NPs. This multifunctional nanoparticle could play an important role in facilitating simultaneously imaging and PTT to achieve better therapeutic efficacy.

Keywords: Targeted photothermal therapy, Photoacoustic imaging, Polyaniline, Phospholipids, Hybrid nanoparticles, Near-infrared light

1. Introduction

Photothermal therapy (PTT) using light-absorbing agents to convert the NIR light into heat to burn cancer cells has attracted great attention in recent years as a promising approach for cancer treatment.[1-3] However, for effective, safe and personalized PTT treatment, it is crucial to identify the location and size of the tumors before therapy, to monitor the in vivo distribution of photothermal agents during therapy and to evaluate effectiveness after therapy with appropriate imaging techniques.[4-6] Therefore, imaging-guided PTT is desired for cancer therapy and those photothermal agents with dual imaging and therapeutic functions have attracted intensive research interests.[7-12]

Compared with other available medical imaging modalities, photoacoustic (PA) imaging is a newly developed noninvasive imaging system, which combines good spectral selectivity of laser light with high resolution and deep penetration of ultrasound imaging.[13-15] It is necessary to administrate PA imaging contrast agents to minimize the attenuation of light intensity and enhance the contrast of images.[16,17] Both PA imaging contrast agents and photothermal agents share the common attribute of strong absorption in NIR region. Therefore, it is undoubted that PA imaging will be the best guidance for PTT in terms of pre-treatment detection, intra-treatment monitor and post-treatment assessment, which can be realized by using the same photothermal agent.

Very recently, organic nanoparticles, such as porphysome and conjugated polymer nanoparticles based on polyaniline (PANI), polypyrrole (PPy), and

poly-(3,4-ethylenedioxythio-phene):poly(4-styrenesulfonate) (PEDOT:PSS) have been reported to act as photothermal agents, showing promising cancer ablation effect both in vitro and in vivo.[18-25] Among these conjugated polymers, PANI is the oldest and potentially most useful conductive polymer due to its outstanding physicochemical properties and low cost.[26] Moreover, PANI is non-cytotoxic and has been widely used as the PTT agent for photothermal treatment of cancer in vitro and in vivo.[27, 28] However, there is still no report about that the PANI nanoparticles can be used as PA imaging contrast agents to guide photothermal treatment.

In this study, we first successfully demonstrated a folic acid ligand conjugated Lipid-polyaniline hybrid nanoparticle (FA-Lipid-PANI NP) which could simultaneously act as targeted PA and thermal theranostics for cancer diagnosis and treatment in living mice. What's more, we introduced a method of preparing hybrid PANI nanoparticles combined emeralidine salt (ES) PANI doped by dodecylbenzene sulfonic acid (DBSA) with the phospholipids, which was conceptually distinct from other technologies reported up to the present. In order to further improve the cancer selectivity, folic acid (FA) as the targeting ligand was conjugated on the surface of Lipid-PANI NPs to obtain the FA-Lipid-PANI NPs (Figure 1a and b). Hence, the hybrid FA-Lipid-PANI NPs exhibited some unique advantages. (1) Biosafety: FA-Lipid-PANI NP was nontoxic and biodegradable by using the biocompatible lipids as coating agents for intravenous administration. (2) Tumour targeting: FA-Lipid-PANI NPs possesed both passive and active tumor-targeting abilities via enhanced permeability and retention (EPR) effect and folic receptor-mediated

transcytosis, respectively. (3) Theranostics: FA-Lipid-PANI NPs could be simultaneously used as PA imaging contrast agents and photothermal agents for tumor theranostics (Figure 1c).

2. Experimental Section

Details of the materials used, syntheses, and analysis and characterization methods are provided in the Supporting Information.

3. Results and Discussion

In our strategy, PANI was synthesized by using anilinium salts protonated by hydrochloride (HCl) and ammonium persulfate as an oxidant.[29] The chemical oxidative polymerization process was carried out for 6 hours at 4 ℃ and resulted in a dark-green precipitate, which was purified by washing with copious amounts of deionized water. The synthesized dark-green precipitate was dedoped by sodium hydroxide to obtain a polymer powder of emeralidine base (EB) PANI which had the purple color. The molecular weight of synthesized EB PANI was 5500 Da, as measured by gel permeation chromatograpy (polydispersity index: 1.1). Then, the synthesized EB PANI was dissolved in chloroform and re-doped by DBSA to obtain the ES PANI (dark-green solution) with the long chain alkyl group. When PANI and 1,2-dipalmitoyl-sn-glycero-3-phosphatidylcholine (DPPC) dissolved chloroform solution was evaporated, the obtained film would exhibit a phase-separated morphology due to immiscibility between the hydrophobic PANI and the hydrophilic polar heads of the phospholipids. Furthermore, the long alkyl tail of the phospholipid could be gathered together with the long chain alkyl group of ES PANI.

After adding the phospholipids, the phase-separated thin film of ES PANI and phospholipids was prepared by evaporating the chloroform. The thin film was broken by ultrasonication after adding water to form Lipid-PANI NPs. The obtained NPs were highly water-soluble (Figure 2a) and very stable in the aqueous phase for photothermal application (Figure S1 in the Supporting Information). Transmission electron microscopy (TEM) images showed that Lipid-PANI NPs had smooth surface and spherical shape (Figure 2b), with a diameter size of 120.6 ± 5.2 nm (Figure 2c). After the conjugation with FA, there were no significant changes in the mean size, polydispersity index (PDI) and zeta potential (Table S1 in the Supporting Information). Infrared (IR) spectra of EB PANI，ES PANI, and Lipid-PANI NPs evidenced the adulteration of DBSA on the surface of PANI and the existence of PANI in the final product (Figure S2 in the Supporting Information). Moreover, the absorption properties of EB PANI, ES PANI and Lipid-PANI NPs were further investigated by UV-vis-NIR spectroscopy. In the absorption spectra of EB PANI, a charge transfer between quinoid and benzenoid rings was observed at 550 nm (Figure 2d).[30] When EB PANI was doped with DBSA (transition to ES PANI), the main absorption peak of charge transfer between quinoid and benzenoid rings was red-shifted as a result of increased electron-delivery efficiency. The π–π* transition of ES PANI was analogous to that of EB PANI (550 nm), but charge transfer between quinoid and benzenoid rings was observed in the NIR region (750 nm).[25] Interestingly, when the ES PANI was prepared as Lipid-PANI NPs with phospholipids, the absorption peak of charge transfer was further red-shifted since

that the Lipid-PANI NPs exhibited strong absorbance in the NIR region (810nm). These results indicated that the Lipid-PANI NPs were well-suited as photothermal agent and PA imaing contrast agent for use upon NIR laser irradiation at 810 nm.

We next investigated the photothermal effect of Lipid-PANI NPs compared with pure water. Experimentally, we examined the temperature increase as a function of 1 mL Lipid-PANI NPs aqueous solution (PANI, 0.1 mg ml^{-1}) under NIR laser irradiation (808 nm, 2 W cm^{-2}) for 5 min. The temperature of each studied group was real-time recorded by temperature gauge or IR thermal camera. Following exposure to NIR light, the temperature of the Lipid-PANI NPs increased rapidly and reached a plateau value of approximately 60℃ within 5 min (Figure 2e). In comparison, the temperature of the pure water only increased by roughly 8 ℃. Furthermore, thermal images also confirmed the photothermal effect by observing an obvious color change from purple (pure water) to yellow (solution of Lipid-PANI NPs). Finally, we collected four temperature rising (laser on) and cooling (laser off) curves of the Lipid-PANI dispersion with concentration of 0.2 mg mL^{-1} (Figure 2f). As shown in Figure 2f, no significant decrease for the temperature elevation was observed after four repeated laser on-and-off cycles. These experimental results indicated that the Lipid-PANI NPs with high photothermal conversion efficiency and photostability could be used as the photothermal materials.

To explore the application of Lipid-PANI NPs in biomedicine, we first tested their potential toxicity by performing methyl thiazolyl tetrazolium (MTT) assay on Hela cells. Encouragingly, no significant cytotoxicity of hybrid Lipid-PANI NPs was

observed by Lipid-PANI NPs and FA-Lipid-PANI NPs, even the concentration reached 100 μg mL^{-1} after incubation for 24 h (Figure 3a). The efficacy of photothermal therapy was then evaluated by incubating Hela cells with both Lipid-PANI NPs and FA-Lipid-PANI NPs following the exposure to 808 nm laser. As expected, the viability of cells under laser irradiation was decreased as the concentration of the NPs increased (Figure 3a). The killing efficacy could reach nearly 70% when the FA-Lipid-PANI NPs concentration was 100 μg mL^{-1}. However, the cells incubated with Lipid-PANI NPs showed lower killing efficacy than FA-Lipid-PANI NPs under the 808 laser irradiation. To further investigate cellular uptake of these NPs, FITC (fluorescein isothiocyanate)-labeled NPs were co-incubated with Hela cells at the same PANI concentration. In addition, to confirm the high efficacy of photothermal ablation of cancer cells, the cells were co-stained by 4'-6-diamidino-2-phenylindole (DAPI) and propidium iodide (PI). The fluorescent images were shown in Figure 3b and c. The cells incubated with Lipid-PANI NPs and FA-Lipid-PANI NPs under the laser irradiation showed a large amount of apoptosis or necrosis compared with the control group. In the three samples, the largest quantity of NPs was uptaken after treated with FITC-labeled FA-Lipid-PANI NPs by the mediating of FA ligand, leading to the largest amount of apoptosis. In contrast, little PI fluorescence was observed after Hela cells were treated with Lipid-PANI NPs alone, indicating that cells were not damaged by Lipid-PANI NPs in the absence of NIR irradiation. This was in good agreement with the published report that temperature higher than 50 ℃ could evoke irreversible

cell damage and necrosis.[21]

Based on the in vitro results, we next examined the Lipid-PANI NPs for PA imaging in vivo. Initially, we investigated the feasibility of Lipid-PANI NPs for in vivo PA imaging, in which Hela tumor-bearing Balb/C mice were selected as the animal model. Animal experiments were approved by the China Committee for Research and Animal Ethics in compliance with the law on experimental animals. When the tumors reached approximately 60 mm^3, the mice were treated with intravenous (i.v.) injections of FA-Lipid-PANI NPs (200 μL, 1 mg mL^{-1}). As shown in Figure 4a, compared to pre-injection images, PA signals at 2 h post-injection were detected in the superficial area of the tumor, attributing to the accumulation of NPs in the blood vessel around the superficial area of the tumor. At 6 h post-injection, PA signals induced by FA-Lipid-PANI NPs further increased (Figure 4b). At 24 h post-injection, the PA signals decreased slightly while appearing in the whole tumor region, indicating the deeply penetration of FA-Lipid-PANI into the inner tumor region.

We further investigated the in vivo therapeutic effect of Lipid-PANI NPs. Three groups (five mice per group) of Hela tumor-bearing Balb/C mice were used in our experiment. The saline, Lipid-PANI NPs, or FA-Lipid-PANI NPs solutions were administered by a single tail intravenous injection, respectively. After 6 h, the tumors were irradiated by the NIR laser (808 nm, 2 W cm^{-2}, 5 min). We next monitored the temperature changes in those areas of tumors. The whole body temperature distribution images of mice induced by NIR laser were investigated

using the IR thermal camera. As shown in Figure 4c, upon the 808 nm laser irradiation, the local tumor temperature of the FA-Lipid-PANI NPs injected group rapidly increased to approximate 50 ℃, which was high enough to ablate the tumor cells. While the temperature of Lipid-PANI NPs treated mice increased to less than 43 ℃ under the same irradiation condition. For the control group, the tumor temperature of saline injected mice exhibited no significant increase (below 37 ℃) after laser irradiation. In addition, the tumor sections collected from mice in different groups were stained by DAPI and observed by a CLSM to explore the Lipid-PANI NPs distribution in tumor site. After treatment with FITC-labeled FA-Lipid-PANI NPs, significant fluorescence intensity of FITC was observed in the region of the tumor compared to saline and Lipid-PANI NPs treated group (Figure 4d and Figure S3 in the Supporting Information). Furthermore, the tumor tissues were collected after 1 day for hematoxylin and eosin (H&E) staining studies (Figure 4e). In the FA-Lipid-PANI NPs plus irradiation group, condensation of chromatins and fragmentations of nuclear could be found in the tumor tissues, indicating the intensive necrosis or apoptosis of the cancer cells. In comparison, the tumor cells in the control groups largely retained their normal morphology with distinctive membrane and nuclear structures. Moreover, H&E stained images of main organs of FA-Lipid-PANI NPs treated mice (collected 10 d after injection) indicated no appreciable abnormality or noticeable organ damage (Figure S4 in the Supporting Information). Upon NIR irradiation at 2 W cm^{-2} for 5 min, the tumors of the mice treated with FA-Lipid-PANI NPs shrank during the first four days. On the tenth day,

the tumors were completely eliminated, leaving the original tumor site with black scars (Figure S5 in the Supporting Information). These results indicated that FA-Lipid-PANI NP has great potential to use as a target photothermal agent for effective tumor therapy.

4. Conclusions

In summary, FA-Lipid-PANI NPs which were prepared from phase-separated films of PANI and DPPC by breaking the films with ultra-sonication in water for cancer diagnosis and treatment, were reported for the first time. The resulting Lipid-PANI-assembled NP could be used as used as the active agents in PA imaging-guided PTT. With biocompatible DPPC coating, Lipid-PANI NPs were stable in physiological environments and showed little toxicity to Hela cells at all the tested concentrations. The cancer cell ablation effect under the NIR laser was observed in the in vitro experiments. Moreover, the FA-Lipid-PANI NPs, which were prepared by the appropriate surface conjugation with FA ligand, had achieved the tumor-targeted PTT effect after systemic administration. The FA-Lipid-PANI NPs could thus be used as targeted photothermal agents employing by NIR light. Due to the thermosensitive property of DPPC,[31] it was expected that the further combination with chemotherapy by loading the therapeutic drugs, might offer great opportunities in the development of new cancer therapeutic approaches. Further studies were ongoing in our laboratory to realize PA imaging-guided cancer thermo-chemo therapy using these photothermal hybrid NPs upon systemic administration.

Acknowledgments

The Application Foundation and Cutting-edge Technologies Research Project of Tianjin (Young Program) (15JCQNJC13800) and the National Basic Research Project (973 Program) of China (2014CB932200) are acknowledged for financial support. We thank Associate Professor Jun Dai for providing us the Hela cells.

References

[1] S. Lal, S. E. Clare, N. J. Halas, *Acc. Chem. Res.* **2008**, *41*, 1842.

[2] M. P. Melancon, M. Zhou, C. Li, *Acc. Chem. Res.* **2011**, *44*, 947.

[3] X. H. Huang, P. K. Jain, I. H. El-Sayed, M. A. El-Sayed, *Lasers Med. Sci.* **2008**, *23*, 217.

[4] M. K. Yu, D. Kim, I. H. Lee, J. S. So, Y. Y. Jeong, S. Jon, *Small* **2011**, *7*, 2241.

[5] C. L. Peng, Y. H. Shih, P. C. Lee, T. M. Hsieh, T. Y. Luo, M. J. Shieh, *ACS Nano* **2011**, *5*, 5594.

[6] K. Yang, L. Hu, X. Ma, S. Ye, L. Cheng, X. Shi, C. Li, Y. Li, Z. Liu, *Adv. Mater.* **2012**, *24*, 1868.

[7] Gobin, A. M.; Lee, M. H.; Halas, N. J.; James, W. D.; Drezek, R. A.; West, J. L. *Nano Lett*. **2007**, *7*, 1929.

[8] J. W. Kim, E. I. Galanzha, E. V. Shashkov, H. M. Moon, V. P. Zharov, *Nat. Nanotechnol*. **2009**, *4*, 688.

[9] M. Zhou, R. Zhang, M. Huang, W. Lu, S. Song, M. P. Melancon, M. Tian, D. Liang, C. Li, *J. Am. Chem. Soc.* **2010**, *132*, 15351.

[10] H. Ke, J. Wang, Z. Dai, Y. Jin, E. Qu, Z. Xing, C. Guo, X. Yue, J. Liu, *Angew.*

Chem. Int. Ed. **2011**, *50*, 3017.

[11] T. D. MacDonald, T. W. Liu, G. Zheng, *Angew. Chem. Int. Ed.* **2014**, *27*, 7076.

[12] J. Yu, C. Yang, J. Li, Y. Ding, L. Zhang, M. Z. Yousaf, J. Lin, R. P a n g, L. Wei, L. Xu, F. Sheng, C. Li, G. Li, L. Zhao, Y. Hou, *Adv. Mater.* **2014**, *26*, 4114.

[13] X. Wang, Y. Pang, G. Ku, X. Xie, G. Stoica, L. V. Wang, *Nat. Biotechnol.* **2003**, *21*, 803.

[14] M. Xu, L. V. Wang, *Rev. Sci. Instrum.* **2006**, *77*, 041101.

[15] L. V. Wang, S. Hu, *Science* **2012**, *335*, 1458.

[16] W. Li, P. K. Brown, L. V. Wang, Y. Xia, *Contrast Media Mol. I* **2011**, *6*, 370.

[17] S. K. Maji, S. Sreejith, J. Joseph, M. Lin, T. He, Y. Tong, H. Sun, S. W. K. Yu, Y. Zhao, *Adv. Mater.* **2014**, *26*, 5633.

[18] L. Xu, L. Cheng, C. Wang, R. Peng, Z. Liu, *Polym. Chem.* **2014**, *5*, 1573.

[19] Zhou, Z. Lu, X. Zhu, X. Wang, Y. Liao, Z. Ma and F. Li, *Biomaterials*, **2013**, *34*, 9584.

[20] B-P. Jiang, L. Zhang, Y. Zhu, X-C. Shen, S-C. Ji, X-Y. Tan, L. Cheng, H. Liang, *J. Mater. Chem. B*, **2015**, *3*, 3767.

[21] C. Hsiao, E. Chuang, H. Chen, D. Wan, C. Korupalli, Z. Liao, Y. Chiu, W. Chia, K. Lin, H. Sung, *Biomaterials* **2015**, *56*, 26.

[22] C. Wang, H. Xu, C. Liang, Y. Liu, Z. Li, G. Yang, L. Cheng, Y. Li, Z. Liu, *ACS Nano*, **2013**, *7*, 6782.

[23] Y. Wang, Yun. Xiao, R. Tang, *Chem. Eur. J.* **2014**, *20*, 11826.

[24] Z. Zha, X. Yue, Q. Ren, Z. Dai, *Adv. Mater.* **2013**, *25*, 777.

[25] L. Cheng, K. Yang, Q. Chen, Z. Liu, *ACS Nano*, **2012**, *6*, 5605.

[26] D. Li, J. Huang, R. B. Kaner, *Acc. Chem. Res.* **2009**, *42*, 135.

[27] C. Hsiao, H. Chen, Z. Liao, R. Sureshbabu, H. Hsiao, S. Lin, Y. Chang, H. Sung, *Adv. Funct. Mater.* **2015**, *25*, 721.

[28] J. Shi, Y. Chen, Q.Wang, Y. Liu, *Adv. Mater.* **2010**, *22*, 2575.

[29] J. Yang, J. Choi, D. Bang, E. Kim, E. Lim, H. Park, J. Suh, K. Lee, K. Yoo, E. Kim, Y. Huh, S. Haam, *Angew. Chem. Int. Ed.* **2011**, *50*, 461.

[30] A. J. Heeger, *Chem. Int. Ed.* **2001**, *40*, 2591.

[31] T. Ta, T. M. Porter, *J. Control. Release* **2013**, *169*, 112.

Figure captions

Figure 1. a) A scheme showing the preparation of ES PANI from EB PANI and the chemical structure of DPPC. b) Schematic illustration to show the synthesis of FA-Lipid-PANI NPs. c) Illustration of the photoacoustic imaging guided photothermal therapy using the FA-Lipid-PANI NPs.

Figure 2. a) Solubility test of Lipid-PANI NPs (left) and ES PANI (right) in chloroform (lower phase) and water (upper phase). b) TEM image of Lipid-PANI NPs (scale bar = 0.2 μm). c) Size distribution of Lipid-PANI NPs. d) UV-Vis-NIR absorption spectra of Lipid-PANI NPs dispersed in water, ES PANI and EB PANI dissolved in chloroform. e) Temperature evolution curves and photothermal images of pure water and aqueous solution of Lipid-PANI NPs over a period of 5 min following exposure to the NIR laser (808 nm, 2 W cm^{-2}). f) Temperature monitoring of a Lipid-PANI aqueous suspension at the concentration of 0.2 mg/mL during for successive cycles of an on-and-off laser.

Figure 3. a) Cell viability studies by MTT assay for Hela cells after incubation with various concentrations of Lipid-PANI NPs and FA-Lipid-PANI NPs with or without NIR laser for 24 h, respectively. The data are shown as mean ± standard deviation (SD). Error bars are based on at least triplicate measurements; * $P < 0.05$, ** $P < 0.01$. b) Confocal fluorescence images of DAPI/ PI stained Hela cells with or without FITC-labeled Lipid-PANI NPs incubation after being exposed to the 808 nm laser at 2 W cm^{-2} (scale bar = 25 μm). Blue, red and green colors in the images are represented DAPI-stained nuclear fluorescence, PI-stained dead cell fluorescence and FITC-labeled Lipid-PANI NPs fluorescence, respectively. c) Confocal fluorescence images of DAPI / PI stained Hela cells with and without Lipid-PANI NPs incubation after being exposed to the 808 nm laser at 2 W cm^{-2}(scale bar = 100 μm). Blue and purple colors represented live and dead cells, respectively.

Figure 4. a) PA images, ultrasound (US) images, and overlaid PA (red) and US images (grey) of Hela tumor (region enveloped by yellow dotted line) before and after tail vein injection of 200 μL of FA-Lipid-PANI NPs (1 mg ml^{-1}) in living mice (excitation wavelength = 808 nm for PA imaging). d) Quantitative analysis of PA intensity obtained from Hela tumor images before and after injection with FA-Lipid-PANI NPs in living mice (n = 3). c) Photothermal images and the 3D temperature distribution of tumor-bearing nude mice that exposed to the NIR laser irradiation (808 nm, 2 W cm^{-2}, 5min). b) In vivo distribution of Lipid-PANI NPs and FA-Lipid-PANI NPs in nude mice bearing Hela tumors 6 h post treatment. d) Histological analysis of Lipid-PANI NPs distribution in tumors post various

treatments (scale bar = 50 μm). Blue and green colors in the images are represented DAPI-stained nuclear fluorescence and FITC-labeled Lipid-PANI NPs fluorescence, respectively. e) H&E-stained tumor slices collected from mice post various treatments (scale bar = 25 μm).

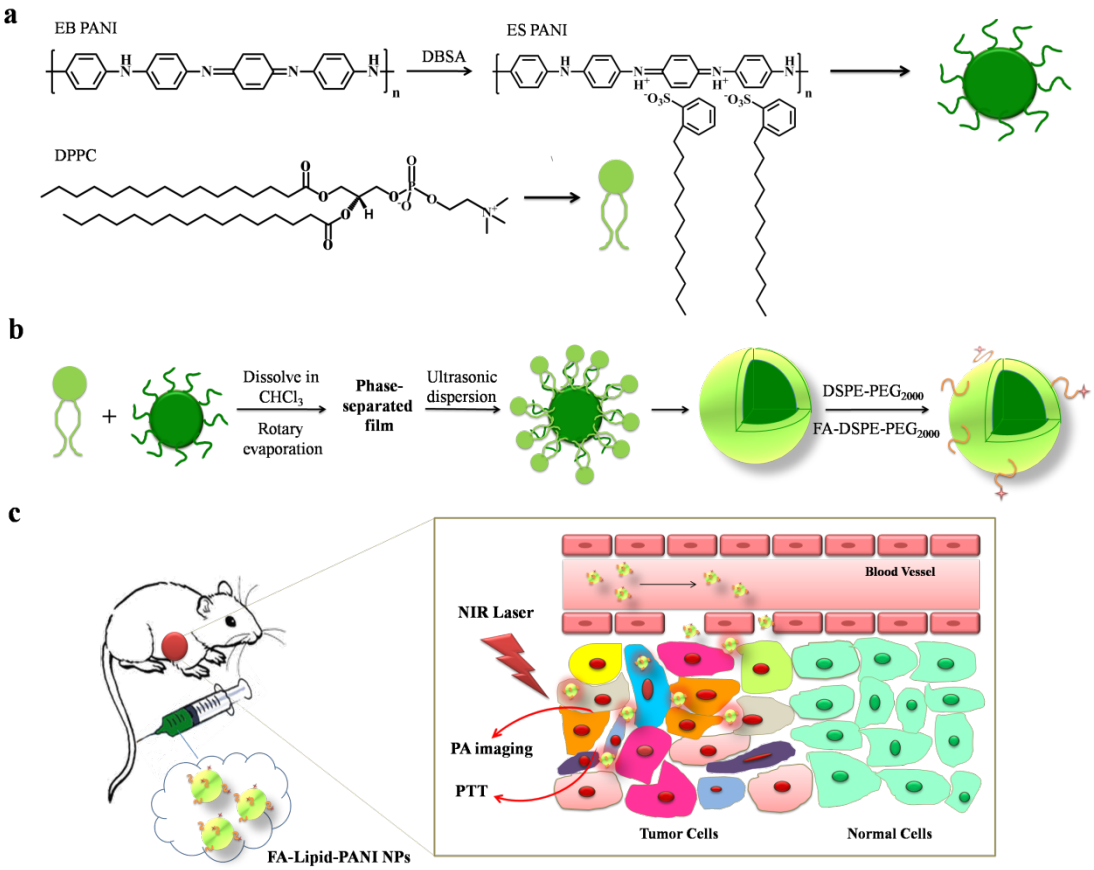

Figure 1. a) A scheme showing the preparation of ES PANI from EB PANI and the chemical structure of DPPC. b) Schematic illustration to show the synthesis of FA-Lipid-PANI NPs. c) Illustration of the photoacoustic imaging guided photothermal therapy using the FA-Lipid-PANI NPs.

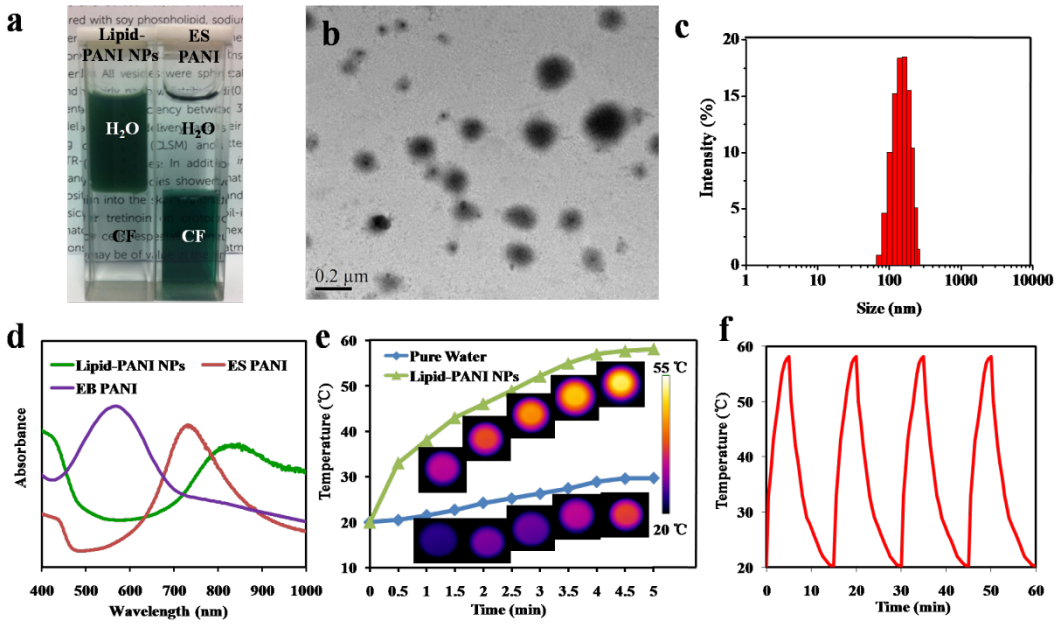

Figure 2. a) Solubility test of Lipid-PANI NPs (left) and ES PANI (right) in chloroform (lower phase) and water (upper phase). b) TEM image of Lipid-PANI NPs (scale bar = 0.2 μm). c) Size distribution of Lipid-PANI NPs. d) UV-Vis-NIR absorption spectra of Lipid-PANI NPs dispersed in water, ES PANI and EB PANI dissolved in chloroform. e) Temperature evolution curves and photothermal images of pure water and aqueous solution of Lipid-PANI NPs over a period of 5 min following exposure to the NIR laser (808 nm, 2 W cm^{-2}). f) Temperature monitoring of a Lipid-PANI aqueous suspension at the concentration of 0.2 mg/mL during for successive cycles of an on-and-off laser.

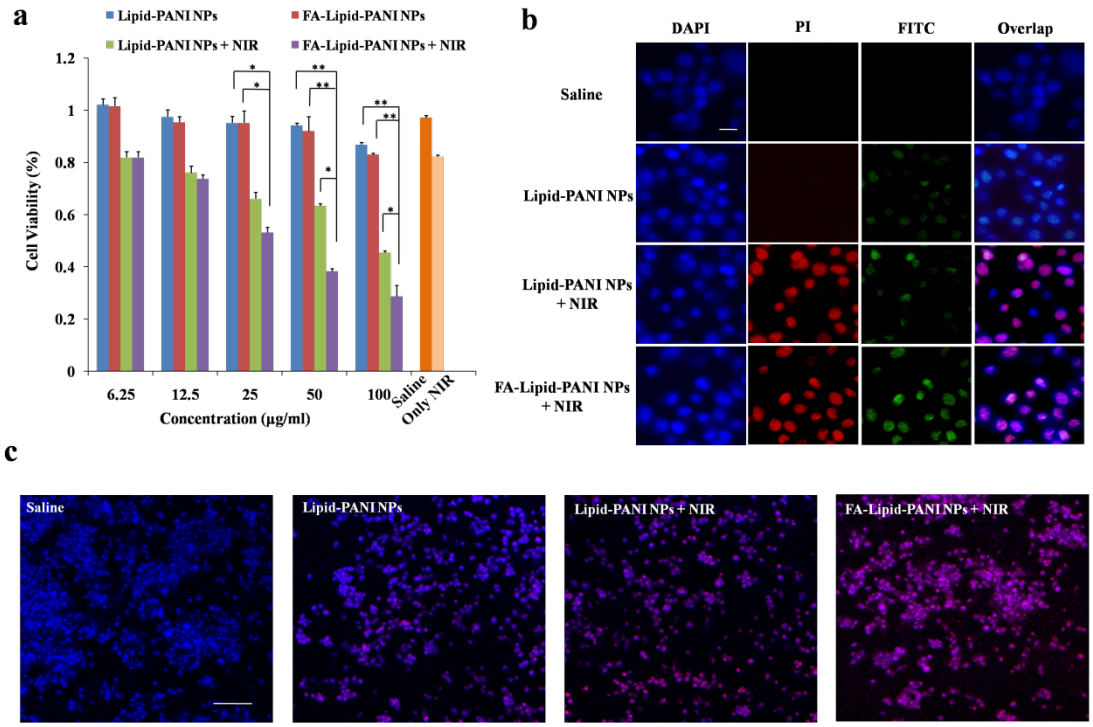

Figure 3. a) Cell viability studies by MTT assay for Hela cells after incubation with various concentrations of Lipid-PANI NPs and FA-Lipid-PANI NPs with or without NIR laser for 24 h, respectively. The data are shown as mean ± standard deviation (SD). Error bars are based on at least triplicate measurements; * $P < 0.05$, ** $P < 0.01$. b) Confocal fluorescence images of DAPI/ PI stained Hela cells with or without FITC-labeled Lipid-PANI NPs incubation after being exposed to the 808 nm laser at 2 W cm^{-2} (scale bar = 25 μm). Blue, red and green colors in the images are represented DAPI-stained nuclear fluorescence, PI-stained dead cell fluorescence and FITC-labeled Lipid-PANI NPs fluorescence, respectively. c) Confocal fluorescence images of DAPI / PI stained Hela cells with and without Lipid-PANI NPs incubation after being exposed to the 808 nm laser at 2 W cm^{-2}(scale bar = 100 μm). Blue and purple colors represented live and dead cells, respectively.

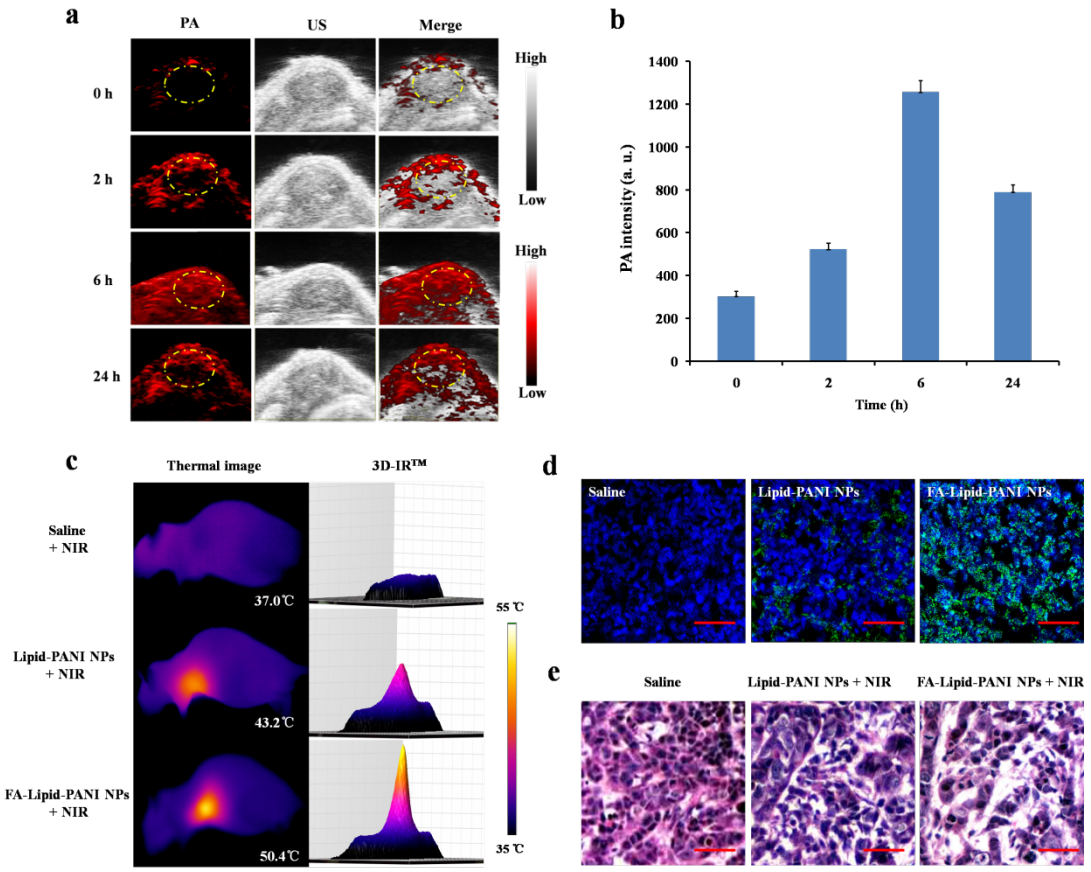

Figure 4. a) PA images, ultrasound (US) images, and overlaid PA (red) and US images (grey) of Hela tumor (region enveloped by yellow dotted line) before and after tail vein injection of 200 μL of FA-Lipid-PANI NPs (1 mg ml^{-1}) in living mice (excitation wavelength = 808 nm for PA imaging). b) Quantitative analysis of PA intensity obtained from Hela tumor images before and after injection with FA-Lipid-PANI NPs in living mice (n = 3). c) Photothermal images and the 3D temperature distribution of tumor-bearing nude mice that exposed to the NIR laser irradiation (808 nm, 2 W cm^{-2}, 5min). d) Histological analysis of Lipid-PANI NPs distribution in tumors post various treatments (scale bar = 50 μm). Blue and green colors in the images are represented DAPI-stained nuclear fluorescence and FITC-labeled Lipid-PANI NPs fluorescence, respectively. e) H&E-stained tumor

slices collected from mice post various treatments (scale bar = 25 μm).